Intra-miniband gain in a super-superlattice structure with alternating electric-field domains

L. Schrottke, M. Giehler, and H. T. Grahn

Citation: Journal of Applied Physics **101**, 036101 (2007); doi: 10.1063/1.2430782
View online: http://dx.doi.org/10.1063/1.2430782
View Table of Contents: http://scitation.aip.org/content/aip/journal/jap/101/3?ver=pdfcov
Published by the AIP Publishing

Intra-miniband gain in a super-superlattice structure with alternating electric-field domains

L. Schrottke,[a] M. Giehler, and H. T. Grahn
Paul-Drude-Institut für Festkörperelektronik, Hausvogteiplatz 5–7, 10117 Berlin, Germany

(Received 2 August 2006; accepted 17 November 2006; published online 1 February 2007)

A super-superlattice structure containing a conventional superlattice, a graded-gap superlattice, and a wide quantum well in its unit cell is analyzed. It is designed in such a way that alternating high- and low-electric-field domains appear due to the presence of positive and negative space charges. The positive space charge is formed by ionized donors, while electrons, which are trapped in the wide quantum well, provide the negative space charge. Since the low-field domain spans the conventional superlattice and the high-field domain is located in the graded-gap superlattice, the flatband condition can be simultaneously achieved for the two superlattices. The self-consistent solution of the Poisson and Schrödinger equations using a simplified scattering-rate approach demonstrates that the conventional superlattice exhibits an inversion of the intra-miniband population. Such structures may be useful for terahertz lasers, since the large dipole matrix element of the intra-miniband transitions allow for a rather low doping density and hence a reduction of scattering processes. Furthermore, they permit the study of superlattices under flatband conditions with a nonequilibrium population, which is achieved without optical excitation. © *2007 American Institute of Physics*. [DOI: 10.1063/1.2430782]

About 7 years before Faist *et al.*[1] demonstrated the operation of quantum-cascade lasers (QCLs), Yuh *et al.*[2] had proposed a so-called infrared band-aligned superlattice laser. According to Yuh's idea, the device consists of three superlattices (SLs). The SL in the center (SL II according to Fig. 1 of Ref. 2) is designed to provide the lasing transition between two minibands. While SL I exhibits only one miniband, which is aligned with the upper miniband of SL II, the two minibands of SL III are arranged in such a way that the lower miniband of SL III is aligned with the lower one of SL II. At the same time, the upper miniband of SL III is above the upper miniband of SL II. In order to inject carriers from the contacts into SL I and to maintain the flatband condition for the SLs, the structure has to be doped with the highest doping density in region I. However, the doping profile is expected to modify the internal distribution of the electric field so that the flatband condition cannot be guaranteed without taking into account the carrier distribution. Furthermore, dopants in the optically active region II may lead to additional scattering processes so that the lasing process must compete with enhanced nonradiative transitions. These difficulties seem to be the major reasons why a successful demonstration of a band-aligned SL laser has not yet been reported.

In 1998, Tredicucci *et al.*[3] demonstrated the operation of a QCL using a superlattice structure with separated positive and negative space charges. The gain was attributed to an inter-miniband transition in the intrinsic superlattice. However, some doubt about the source of the gain remains, since, due to the large dipole matrix elements of the inter-miniband transitions, an extremely fast carrier injection into the upper miniband is necessary. We believe that the gain is due to the transition g-1 (bound-to-continuum) rather than the inter-miniband transition 2-1 (using the notation of Ref. 3). The designs of various kinds of QCLs (Ref. 4) with an undoped active region reveal that a rather complicated scheme of coupled subbands is required for efficient electron injection in such structures. Furthermore, Kleinert and Bryksin[5] showed for conventional SLs under bias that two minibands are not sufficient for an intrinsic population inversion. Therefore, three minibands are necessary for intrinsic population inversion in conventional SLs.

Recently, the implementation of QCLs has been extended to the terahertz (THz) spectral region. While Köhler *et al.*[6] have reported QCL-like structures with seven quantum wells (QWs), Kumar *et al.*[7] have developed inter-subband lasers with only four or five QWs in each period. In view of these THz sources, the idea of a band-aligned SL laser is analyzed again: If the gap between the involved minibands is sufficiently large to allow for longitudinal-optic (LO) phonon scattering, a very fast population of the upper edge of the lower miniband is possible by inter-miniband transitions. Therefore, an intra-miniband population inversion of the lower miniband and hence gain for the THz spectral region may be achieved, provided that the lower miniband edge is depopulated sufficiently fast. Furthermore, the combination of the flatband condition with a nonequilibrium miniband population would allow investigation of the influence of coherent and incoherent electron transport on the inter- and intra-miniband transitions by varying the SL length.

In this Letter, we present the design and analysis of such a super-superlattice, which contains a conventional SL under flatband condition, a graded-gap SL, and a wide QW in its unit cell. At the same time, this structure exhibits alternating electric-field domains due to the presence of positive and negative space charges. The analysis is based on the

[a]Electronic mail: lutz@pdi-berlin.de

Schrödinger equation in the envelope function approximation with an effective mass, which depends linearly on energy.[8] For the self-consistent procedure, the corrections of the potential are calculated from the carrier distribution, which is determined in the framework of a simple scattering-rate model, for which *k*-space integration is neglected. The scattering rates are assumed to be proportional to the dipole matrix elements[9] for the respective pairs of states. In order to simulate LO-phonon coupling, the transition rates are also assumed to depend on the transition energy with a significant increase of the rate at 36 meV. For this calculation, the structure is considered to be infinitely long, and all periods are equal. Note, however, that each period consists of many layers as for a conventional QCL structure. In order to improve the convergence behavior of the self-consistent procedure, a self-adjusting convergence factor is applied, which takes into account the magnitude of the potential correction.[10] The details of the numerical procedure are described in Ref. 11.

The presented structure is designed in such a way that the undoped conventional SL is in the low-field domain, while the graded-gap SL is in the high-field domain, i.e., near-flatband condition can simultaneously be achieved for both SLs for a certain applied voltage. The alternating field-domain structure is formed by alternating positive and negative space charges. Using *n* doping, the depletion of donors results in a positive space charge, which is responsible for the potential bending at the transition from the high-field to the low-field domain. This space charge is localized at the position of the doping and is therefore called static boundary charge. In contrast, the electrons are assumed to move through the structure, but are partially trapped in a wide QW so that a negative space charge is formed there. This space charge, which leads to the band bending for the transition from the low-field to the high-field domain, is called dynamic boundary charge. Due to the interplay of the conduction subband structure and the electron distribution, the dynamic boundary charge has to be determined self-consistently. Figure 1 shows the calculated conduction band profile and the wave functions in this structure for an average field strength of 17 kV/cm. The position of the donors is marked by a thick line at the conduction band edge for the QW material. Each period contains three regions similar to the band-aligned SL structure. Region I can be considered as the injector, region II is the optically active SL under flatband condition, and region III serves as the extractor. At the same time, region III forms a transition region to the following period so that this structure can be cascaded in a similar way as QCL structures.

The transition region III operates as an overflow valve for the electrons. For a lower electron density in the widest well, the ground state in the adjacent narrow well (first QW of the graded-gap SL) is higher than the ground state in the widest well, forming an effective barrier. With increasing population in the widest well, its potential is raised so both states become resonantly coupled and limit the population of the widest QW. The challenge for the design is to determine the doping density at which, in both the conventional SL and the graded-gap SL, the minibands are simultaneously formed. Note that our simplified model may underestimate

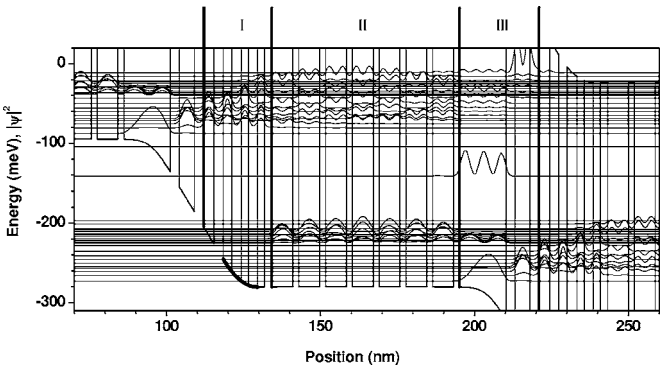

FIG. 1. Conduction band profile and wave functions for the super-superlattice structure with alternating field strengths. For the calculations, the $GaAs/Al_{0.45}Ga_{0.55}As$ materials system is used with a band offset of 442 meV, effective masses of 0.067 and 0.104 for GaAs and $Al_{0.45}Ga_{0.55}As$, respectively, and a nonparabolicity factor $\gamma=4\times10^{-5}$ meV^{-1}. The layer sequence of region I is (in nanometers, bold numbers denote barriers) 3.4, **3.0**, 2.7, **3.2**, 2.3, **3.0**, 2.2, **2.5**. Region II consists of a SL with seven periods of 6.7 and **2.0** nm, while the sequence of region III is 15.0, **3.0**, 4.8, and **3.0**. The boundaries of regions I, II, and III are marked by thick, vertical lines. The thick line at the GaAs conduction band edge denotes the *n*-doped layers with a doping density of 4×10^{17} cm^{-3}, which corresponds to a sheet density of 4.4×10^{11} cm^{-2} per period.

additional scattering processes as well as level broadening and band filling due to the high carrier density in the ground subband of the widest QW. Furthermore, in contrast to the band-aligned SL design, there is no strict blocking of the upper miniband at the boundary between regions II and III. However, this problem may be overcome by an enlargement of the SL length, since Rauch *et al.*[12] have shown that coherent miniband transport in SLs is restricted to only a few periods due to, e.g., interface roughness, so that the electrons may scatter into the lower miniband inside region II rather than into the continuum at the end of this region.

In the framework of our model, the self-consistent calculation allows us to determine the occupation numbers of the subbands, which are considered as separate states, since we restrict our calculations to $k=0$. Therefore, the minibands are represented by quasi-minibands, which consist of a finite number of states. The lower quasi-miniband contains eight states originating from the ground states of the seven QWs of the conventional SL and the first excited state of the wide QW. For the configuration presented in Fig. 1, the calculation shows that about 98% of the electrons are trapped within this wide QW. There is no significant population inversion between the upper and the lower miniband. Only the population of the lowest state of the upper miniband (0.8%), which is rather localized in region I, is larger than the population of the highest state of the lower miniband (0.2%), so that we do not expect a sufficient gain of the inter-miniband transition. In contrast to that, the states within the lower miniband exhibit larger occupation numbers for higher energies. In Fig. 2, the occupation of the eight states representing the lower miniband is shown as a function of the respective subband energies exhibiting clearly an increasing occupation with increasing subband energy. Using the semiempirical approach described in Ref. 11, the scattering times for transitions between adjacent subbands within the lower quasi-miniband are estimated to be between 1.5 and 2 ps. The partial local-

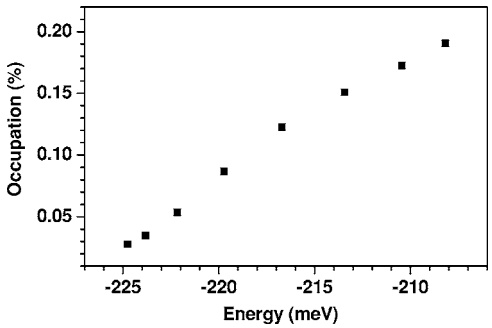

FIG. 2. Occupation numbers of the states representing the lower quasi-miniband of region II in percent of the total number of electrons per period as a function of the respective subband energies. These energies correspond to the energy scale shown in Fig. 1.

ization of the lower states of the upper quasi-miniband leads to inter-miniband transition times of about 1.5 to 7 ps, which are longer than expected for a regular SL. Because direct inter-miniband transitions into the lower states of the lower quasi-miniband are about 2 orders of magnitude slower and the upper edge is populated from several states of the upper miniband, population inversion is formed. This intra-miniband population inversion may lead to gain in the THz spectral region.

In order to estimate the gain, we calculate $\tilde{G}=(N_i-N_j)|D_{ij}|^2$, with N_i and D_{ij} denoting the population of the ith subband and the dipole matrix element, respectively. For more details, see Ref. 11. Although our model allows us to calculate the values only in arbitrary units, the results can be used for comparison with the ones of other THz sources treated with our model. Figure 3 shows the calculated values for $\tilde{G}$ as a function of the intersubband transition energies. The value of the gain maximum at about 3 meV, which corresponds to frequencies just below 1 THz, has for both the gain and the gain coefficient, the same order of magnitude as we have calculated for the structure reported in Ref. 7. Since the calculated emission energy of the super-superlattice is significantly smaller than the lasing energy of about 12 meV reported in Ref. 7, the optical losses may be different. However, reabsorption is included in our model, while the energy dependence of free-carrier absorption can be neglected. For

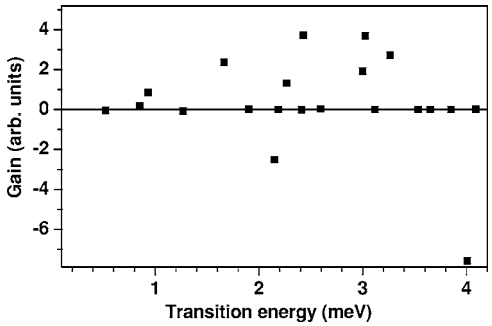

FIG. 3. Calculated gain $\tilde{G}$ as a function of the transition energy for intra-miniband transitions within the lower miniband of the SL.

GaAs with bulk carrier concentrations larger than 2×10^{17} cm^{-3} and photon frequencies below 3 THz, the product of photon frequency and electron relaxation time is smaller than unity so that the Drude model predicts, in agreement with experimental data, an almost frequency-independent absorption coefficient between about 1 and 3 THz due to free-carrier absorption. Furthermore, the energy of the gain maximum can be shifted to higher values using lower and thinner barriers in order to enlarge the miniband width.

An advantage of such a flatband intra-miniband laser is probably the rather large dipole matrix elements, which can even be adjusted by changing the length of the SL. This could allow for a smaller carrier density and therefore for a reduction of the influence of electron-electron scattering. In particular, the quasi-minibands are occupied by less than 2% of the total number of electrons so that the carrier density in the optically active region II is in fact rather small. At the same time, the formation of the domain boundary requires a large doping in order to provide a sufficiently large charge density in region III, but it is spatially separated from region II. A major challenge for this design is the precise adjustment of the doping density, which is necessary in order to achieve the correct band bending for the simultaneous formation of the minibands in both SLs.

In conclusion, we have designed and analyzed a super-superlattice structure containing both a conventional SL and a graded-gap SL, and a QW in which static (dopants) and dynamic boundary charges (in the QW) lead to the formation of an alternating electric-field-domain structure. Self-consistent calculations show that intra-miniband gain is possible within the lower miniband of the conventional SL in the low-field domain. Devices based on this design may be useful for THz lasers.

The authors would like to thank P. Kleinert for stimulating discussions.

[1] J. Faist, F. Capasso, D. L. Sivco, C. Sirtori, A. L. Hutchinson, and A. Y. Cho, Science **264**, 553 (1994).
[2] P. Yuh and K. L. Wang, Appl. Phys. Lett. **51**, 1404 (1987).
[3] A. Tredicucci, F. Capasso, C. Gmachl, D. L. Sivco, A. L. Hutchinson, A. Y. Cho, J. Faist, and G. Scamarcio, Appl. Phys. Lett. **72**, 2388 (1998).
[4] C. Gmachl, F. Capasso, D. L. Sivco, and A. Cho, Rep. Prog. Phys. **64**, 1533 (2001), and references therein.
[5] P. Kleinert and V. V. Bryksin, Phys. Rev. B **63**, 193303 (2001).
[6] R. Köhler, A. Tredicucci, F. Beltram, H. E. Beere, E. H. Linfield, A. G. Davies, D. A. Ritchie, R. C. Iotti, and F. Rossi, Nature **417**, 156 (2002).
[7] S. Kumar, B. S. Williams, S. Kohen, Q. Hu, and J. L. Reno, Appl. Phys. Lett. **84**, 2494 (2004).
[8] Compare, e.g., G. Bastard, *Wave Mechanics Applied to Semiconductor Heterostructures* (Les Éditions de Physique, Les Ulis, 1988), pp. 83–89.
[9] C. Sirtori, F. Capasso, J. Faist, and S. Scandolo, Phys. Rev. B **50**, 8663 (1994).
[10] F. Stern, J. Comput. Phys. **6**, 56 (1970).
[11] L. Schrottke, M. Giehler, R. Hey, and H. T. Grahn, J. Appl. Phys. **100**, 053102 (2006).
[12] C. Rauch, G. Strasser, K. Unterrainer, W. Boxleitner, and E. Gornik, Phys. Rev. Lett. **81**, 3495 (1998).